Electron Thermionic Emission from Graphene and a Thermionic Energy Converter

Shi-Jun Liang and L. K. Ang*

SUTD-MIT International Design Center, Singapore University of Technology and Design, Singapore 138682

(Received 19 May 2014; revised manuscript received 3 September 2014; published 12 January 2015)

In this paper, we propose a model to investigate the electron thermionic emission from single-layer graphene (ignoring the effects of the substrate) and to explore its application as the emitter of a thermionic energy converter (TIC). An analytical formula is derived, which is a function of the temperature, work function, and Fermi energy level. The formula is significantly different from the traditional Richardson-Dushman (RD) law for which it is independent of mass to account for the supply function of the electrons in the graphene behaving like massless fermion quasiparticles. By comparing with a recent experiment [K. Jiang *et al.*, Nano Res. 7, 553 (2014)] measuring electron thermionic emission from suspended single-layer graphene, our model predicts that the intrinsic work function of single-layer graphene is about 4.514 eV with a Fermi energy level of 0.083 eV. For a given work function, a scaling of T^3 is predicted, which is different from the traditional RD scaling of T^2. If the work function of the graphene is lowered to 2.5–3 eV and the Fermi energy level is increased to 0.8–0.9 eV, it is possible to design a graphene-cathode-based TIC operating at around 900 K or lower, as compared with the metal-based cathode TIC (operating at about 1500 K). With a graphene-based cathode (work function = 4.514 eV) at 900 K and a metallic-based anode (work function = 2.5 eV) like LaB_6 at 425 K, the efficiency of our proposed TIC is about 45%.

DOI: 10.1103/PhysRevApplied.3.014002

I. INTRODUCTION

Thermionic emission describes electron evaporation from a heated cathode when the electrons gain sufficient energy from the thermal energy to overcome the potential barrier (or work function) near the cathode surface (see Fig. 1). The amount of current density J from the thermionic emission is determined by the Richardson-Dushman (RD) law [1], given by

$$J = AT^2 \exp\left[-\frac{\Phi}{k_B T}\right]. \tag{1}$$

Here, T is the cathode temperature, Φ is the work function of metal (independent of T), k_B is the Boltzmann constant, the prefactor $A = 4\pi emk_B^2/h^3 = 1.2 \times 10^6\ \mathrm{A\,m^{-2}\,K^{-2}}$ is the Richardson constant, e is the electron charge, and m is the electron mass. In general, the RD law works well only for metallicklike materials, and a corresponding modification using quantum models is required for wide-band-gap materials and low-electron-affinity materials [2].

Since monolayer graphene [3] was exfoliated experimentally in 2004, many unique properties have been reported, such as linear band structure [4], ultrahigh mobility (up to $40\,0000\ \mathrm{cm\,V^{-1}\,s^{-1}}$), and excellent conductivity [5]. Fundamentally, the linear band structure of graphene, the most intriguing property, makes it different from other three-dimensional or bulk materials. For electron emission, it has been recently shown that the traditional emission processes, such as field emission and photoassisted overbarrier electron emission, may require further revisions [6–8] to account for the unique properties of graphene. As the crystalline allotrope of carbon, the thermionic and field emission from carbon nanotubes (CNT) have also been studied both experimentally [9–12] and theoretically [13–15], which indicates that traditional emission models may not be valid for CNT. Recent experiments [16,17] confirm that the RD law is not valid for thermionic emission from CNT.

In this paper, we are interested to know if the RD law [Eq. (1)] is valid for thermionic emission from single-layer suspended graphene by assuming that the effect of the substrate is not important. Electrons in graphene behave as massless quasiparticles ($m = 0$), so the mass-dependent expression of the prefactor A in the RD law [Eq. (1)] is questionable, as the supply function of the electron behaving like massless particles in graphene is not included. On the other hand, the electrons in graphene must exhibit a nonzero mass when they are collectively excited, which is only a few percentage points (0.01–0.03) of the intrinsic electron mass [18].

Harvesting thermal energy is important to maintain sustainable energy needs, since nearly 60% of the energy input to our society is wasted as heat. One of the most common methods in converting heat into electricity is based on thermoelectric (TE) materials, which has progressed significantly since the 1990s by using low-dimensional materials [19]. One of the limitations of TE

*ricky_ang@sutd.edu.sg

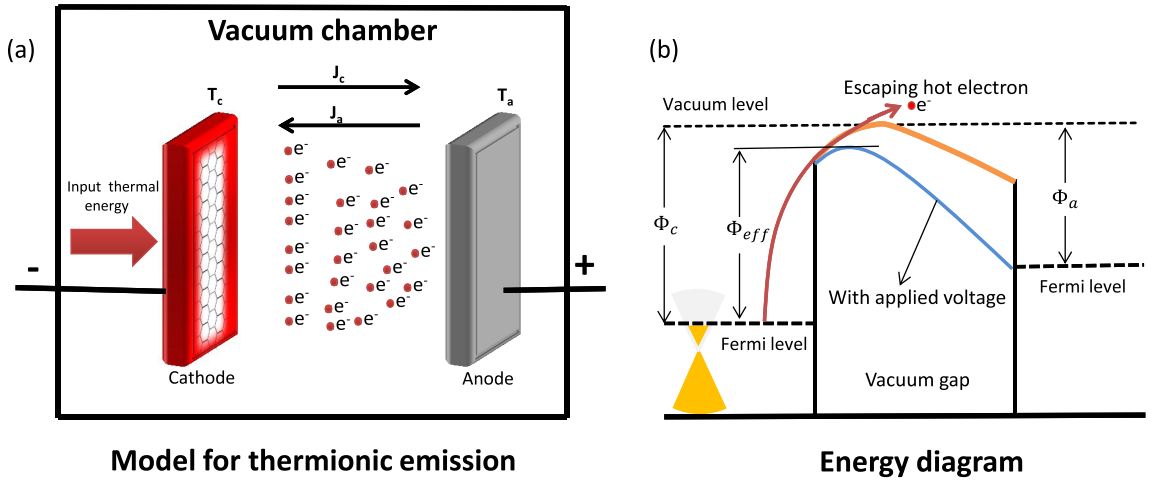

FIG. 1. (a) Schematic diagram of the electron thermionic emission process of a graphene-based TIC, where T_c and T_a are the cathode temperature and anode temperature, respectively; J_c and J_a are the current flow from cathode to anode and from anode to cathode, respectively. (b) The energy level for the TIC shown in (a). Φ_c and Φ_a are the work function of the cathode and of the anode, respectively. Φ_{eff} is the effective barrier height of the cathode due to the Schottky lowering effect. The orange (blue) line represents the potential profile without (with) the Schottky lowering effect. The red line traces the thermionic emission process of a hot electron into vacuum.

power generators is low efficiency ($< 40\%$) in the temperature ranges of 600–1000 K (see Fig. 6 in Ref. [19]). Another method for the conversion of heat to electricity is known as the thermionic energy converter (TIC), for which electrons are evaporated from a heated cathode into a vacuum and then condensed at a cooler anode [20]. Compared with the TE-based converter (TEC), the TIC normally operates at a high temperature (above 1500 K) with higher efficiency ($> 50\%$). However, it is difficult to operate the TIC at a low temperature, as common metallic cathodes having a high work function cannot produce sufficient electron emission at a low temperature.

The other limiting factor of the TIC is the space-charge effects of the electrons traveling across the gap, which have been addressed either by reducing the gap spacing or by using Cs positive ions. Recently, some satisfactory progress has been achieved to avoid this space-charge problem by modifying the electric potential inside the gap [21] or by introducing heterostructures [22].

It is desirable if the TIC can operate with a relatively high efficiency (compared to the TEC) at an immediate temperature ranging from 700 to 1000 K, which may *significantly* complement the ongoing research of the TEC and also alternative energy-harvesting devices in this intermediate temperature range. Some recent approaches to improving the efficiency of the TIC are achieved by using photo-enhanced thermionic emission from a wide-band-gap emitter [23], engineering surface effects [24], and seeking alternative emitters [25].

Other than studying the validity of using the RD law to describe the electron thermionic emission from graphene, we are also interested in exploring if a graphene-based cathode TIC can have better efficiency than a metal-based cathode TIC at a similar operating condition like the same work function. From our model, we first derive an analytic solution [Eq. (8)] for the thermionic emission from graphene, which indicates that the traditional RD law fails to describe thermionic emission from a single suspended layer of graphene [see Fig. 2(a)]. The calculated results are in very good agreement with very recent experimental data [26] [see Fig. 4(a)]. If the property of graphene can be tuned to some favorable parameters, we also predict that the proposed graphene-cathode-based TIC can have a higher current density (> 10 A/m^2) at 700–1000 K (see Fig. 3). Finally, we show that for a graphene-based cathode (work function $= 4.514$ eV) at 900 K and a metallic-based anode (work function $= 2.5$ eV) like LaB_6 at 425 K, the efficiency of our proposed TIC is about 45% [see Fig. 5].

II. THEORETICAL MODEL

In Fig. 1(a), we show the schematic diagram of our model. By assuming that the graphene-based cathode has been heated up to a uniform temperature T_c (without considering the heating process and uniformity issue for simplicity), the electrons will be emitted from the cathode to reach the anode biased at temperature T_a, by overcoming the potential barrier as shown in Fig. 1(b). The work function of the cathode and of anode is, respectively, defined as Φ_c and Φ_a. The amount of the emitted current density from the cathode and anode is, respectively, J_c and J_a, which will be calculated in this paper.

The electron theory of graphene proposed by Wallace [27] can provide the basis for practically all properties of graphene. This theory implies that an electron in graphene mimics the Dirac fermion and that the equation of electron motion obeys the 2D Dirac-like equation. By using this model, the electron state is described by a two-component

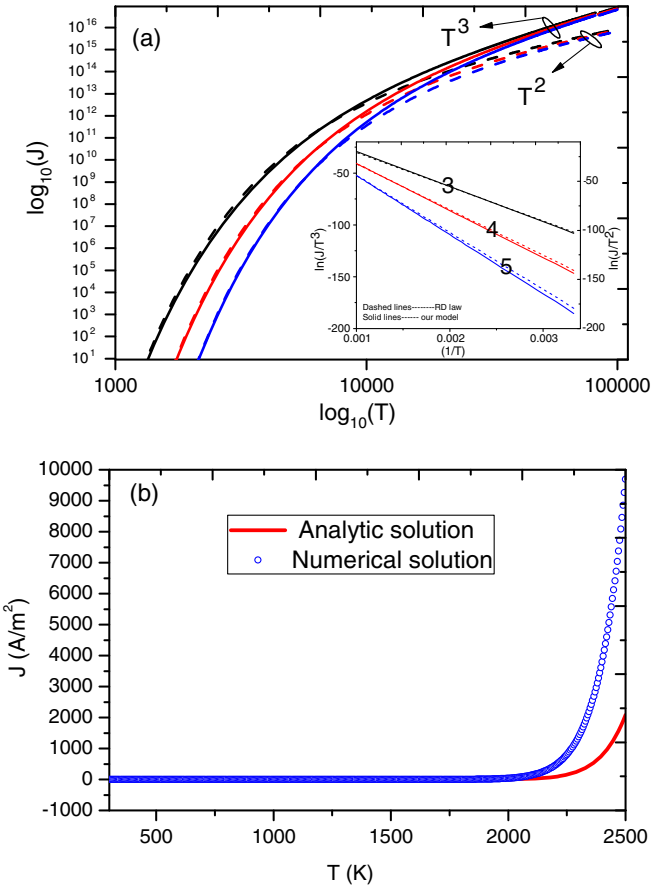

FIG. 2. (a) The emitted current density J (A/m^2) as a function of temperature T (K) for our model (solid lines) and the RD law (dashed lines) at three different work functions Φ (eV) = 3, 4, and 5 (top to bottom). The inset shows $\ln(J/T^3)$ (left y axis) and $\ln(J/T^2)$ (right y axis) versus $1/T$. (b) A comparison of the analytical formula [Eq. (8)] (red line) with the numerical solution of Eq. (7) (circle) as a function of temperature (for $E_F = 0.083$ eV and $\Phi = 4.514$ eV).

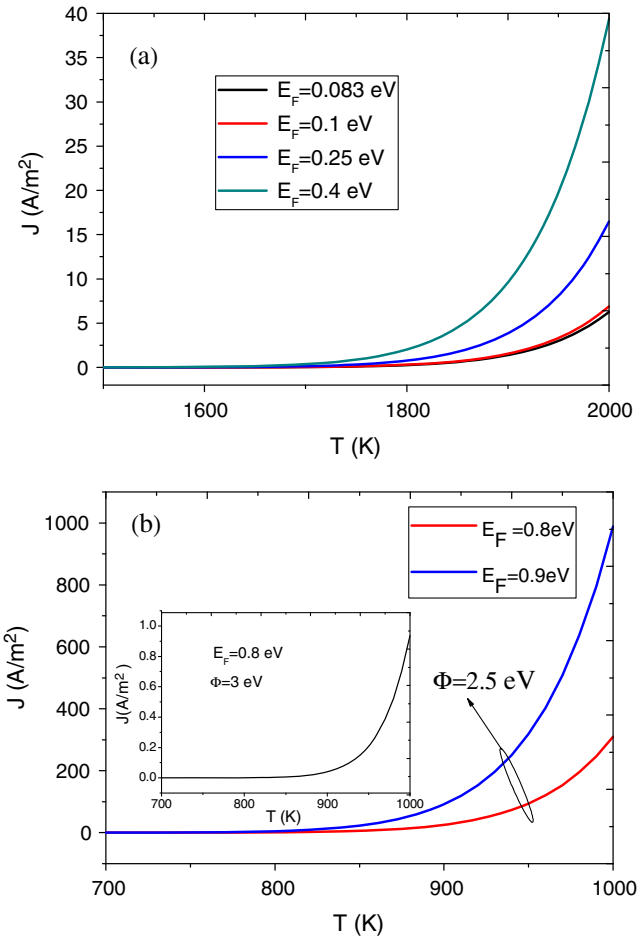

FIG. 3. (a) The current density J as a function of temperature T for various E_F (eV) = 0.083 (intrinsic), 0.1, 0.25, and 0.4 (bottom to top). (b) J as a function of T at higher E_F (eV) = 0.8 and 0.9 and lower Φ (eV) = 2.5 and 3. The inset presents the result at $E_F = 0.8$ eV and $\Phi = 3$ eV with a much lower J.

wave function for which the parallel electron energy is $E_p = \hbar v_f |\mathbf{k}|$ in the low-energy regime. The number of electron states per unit cell with energy between E_p and $E_p + dE_p$ is given by [28]

$$\rho(E_p)dE_p = \frac{2}{(2\pi)^2}\iint d^2k = \frac{2E_p}{\pi(\hbar v_f)^2}dE_p, \qquad (2)$$

where $\hbar$ is the reduced Planck constant and v_f (10^6 m/s) is the velocity of massless Dirac fermions in the graphene. The probability of an electron state with total energy E being occupied is given by the Fermi-Dirac (FD) distribution function

$$f_{\mathrm{FD}}(E) = \frac{1}{1+\exp[(E-E_F)/k_BT]}, \qquad (3)$$

where E_F is the Fermi energy level (= 0.083 eV for intrinsic graphene). The number of electrons (per area and per time) perpendicularly crossing the graphene plane with total energy between E and $E + dE$ and normal energy between E_x and $E_x + dE_x$ is given by

$$N(E,E_x)dEdE_x \equiv \frac{2f_{\mathrm{FD}}(E)}{(2\pi)^2}\iiint_{E,E_x} v_x d^2k dk_x = \frac{1}{\pi\hbar^3 v_f^2}E_p f_{\mathrm{FD}}(E)dE_p dE_x. \qquad (4)$$

In the derivation of Eq. (4), we have assumed that the normal energy component of electrons is $E_x = \hbar^2 k_x^2/2m$. This assumption may be justified by the reasoning that graphene has an atomic thickness for which the electrons are confined in a finite quantum well in the normal direction. The barrier height of the quantum well is assumed to be the intrinsic work function of single-layer graphene, which may be different from bulk graphite. Because of the quantum confinement, we solve the time-independent Schrödinger equation of electrons traveling in

the normal direction to obtain the energy of the ground state, which is E_x as given in the equations above. Using Eq. (4), we calculate the total number of electrons with normal energy between E_x and $E_x + dE_x$ at the equilibrium condition, which gives

$$N(E_x)dE_x = \frac{dE_x}{\pi\hbar^3 v_f^2}\int_{E_x}^{\infty}(E - E_x)f_{\mathrm{FD}}(E)dE. \quad (5)$$

To solve Eq. (5) analytically, we make the following assumptions, which are verified by comparing the analytical result with the numerical calculation as shown in Fig. 2(b). First, we assume that only the electrons with energy greater than or equal to the work function of the cathode (graphene) can be emitted, which means electron tunneling is completely omitted. This assumption is reasonable, as it is the definition of thermionic electron emission. It also implies that only the high-energy component of the Fermi-Dirac distribution is important, for which we may replace the Fermi-Dirac distribution with the Maxwell-Boltzmann distribution $f_{\mathrm{MB}}(E) = \exp[-(E - E_F)/k_BT]$. In doing so, Eq. (5) is simplified to become

$$N(E_x)dE_x = \frac{k_B^2T^2}{\pi\hbar^3 v_f^2}\exp\left[-\frac{E_x - E_F}{k_BT}\right]dE_x. \quad (6)$$

For thermionic emission, the current density of the emitted electrons along the direction perpendicular to the graphene plane is calculated by

$$J(E_F, T) = \int_{\Phi}^{\infty} eN(E_x)dE_x. \quad (7)$$

In solving Eqs. (6) and (7), we obtain an analytical formula for thermionic electron emission from single-layer graphene excluding the effect of substrate, which is

$$J(E_F, T) = \frac{ek_B^3T^3}{\pi\hbar^3 v_f^2}\exp\left[-\frac{\Phi - E_F}{k_BT}\right]. \quad (8)$$

It is clear that Eq. (8) is independent of mass m, solving the inconsistency of the RD law having a finite mass term in the prefactor A, which is troublesome in applying the RD law for electron emission from single-layer graphene. Note that the work function is considered to be temperature independent in our paper. Based on this interesting finding and the importance of electron band structure determining the amount of electron thermionic emission, we speculate that all the materials with linear band structure may have the same scaling law reported here.

It is common that an external and small voltage is used to collect thermionically emitted electrons at the anode. With the applied voltage, the potential barrier is reduced to $\Phi_{\mathrm{eff}} = \Phi - \Delta\Phi$ (due to the Schottky effect) as shown in Fig. 1(b) (dark blue line). Under this situation, the equation is modified as

$$J(E_F, T) = \beta T^3 \exp\left[-\frac{\Phi - E_F - \Delta\Phi}{k_BT}\right], \quad (9)$$

where $\beta = ek_B^3/\pi\hbar^3 v_f^2 = 115.8\ \mathrm{A\,m^2\,K^{-3}}$, $\Delta\Phi = (e^3F/4\pi\epsilon_0)^{1/2}$ represents the reduction in the potential barrier, and F (< 0.1 V/nm) is the electric field [29]. At higher field $F > 1$ V/nm, quantum tunneling begins to dominate over the Schottky emission process, which requires a new model [30], and it will not be addressed in this paper. Throughout this paper, we assume $F = 0$ unless it is specified.

To verify Eq. (8), it is important to have a more realistic surface potential profile $V(x)$ in order to estimate the contribution of electron tunneling through the potential barrier. In doing so, the classical image charge potential V_{im} is arbitrarily included in $V(x)$ (near the cathode), and V_{im} is [31]

$$V_{\mathrm{im}}(x) = -\frac{e^2}{4\pi\epsilon_0}\left[\frac{1}{2x} + \sum_{n=1}^{\infty}\left\{\frac{nD}{(nD^2) - x^2} - \frac{1}{D}\right\}\right], \quad (10)$$

which can be simplified to be [32]

$$V_{\mathrm{im}}(x) = -\frac{1.15\alpha D^2}{x(x - D)}. \quad (11)$$

Here, $\alpha = e^2 \ln 2/8\pi\epsilon_0 D$, D is the gap spacing, and ϵ_0 is the vacuum permittivity. The potential barrier $V(x)$ in between the gap is

$$V(x) = \Phi - V_{\mathrm{im}}(x) = \Phi - \frac{1.15\alpha D^2}{x(x - D)}. \quad (12)$$

Note that the singularities at $x = 0$ and $x = D$ can be avoided by restricting the positive values of x (within $0 < x < D$) to have a positive $V(x)$. This simplified image charge model is verified by using a quantum image charge model [33], and it is valid for $D > 10$ nm.

To determine the effect of electron tunneling through the barrier $V(x)$, we calculate the tunneling probability $D(E_x)$ by solving

$$D(E_x) = \exp\left[-\frac{4\pi\sqrt{2m}}{h}\int_{x_1}^{x_2}\{[V(x) - E_x]\}^{1/2}dx\right] \approx \exp[-\tilde{B}(H - E_x)^{1/2}], \quad (13)$$

where $H = \Phi - 1.15\alpha/b \ln[\frac{(1+b)^2}{(1-b)^2}]$ is the modified barrier height, $b = \sqrt{1 - 4.6\alpha/\Phi}$, and $\tilde{B} = 2(x_2 - x_1)(2m)^{1/2}/h$.

The values of x_1 and x_2 are calculated by solving $V(x) = 0$. The amount of the tunneling current density is calculated by

$$J_T = e\int_0^\infty N(E_x)D(E_x)dE_x \approx \frac{e^{-\tilde{B}H^{1/2}}}{\pi\hbar^3 v_f^2/e}\left[\frac{1}{3}E_F^3 - 2(k_BT)^3\,\mathrm{polylog}\left(3, -e^{-\frac{E_F}{k_BT}}\right)\right], \quad (14)$$

where $\mathrm{polylog}(3, x)$ is the polylogarithm function [34].

In the derivation of Eq. (14), we assume that only electrons around the Fermi level participate in the tunneling process. Based on the default parameters used in our calculation, $E_F = 0.083\,\mathrm{eV}$, $\Phi = 4.514\,\mathrm{eV}$, and $v_f = 10^6\,\mathrm{m/s}$, the term $e^{-\tilde{B}H^{1/2}}$ is nearly zero, which implies that the amount of the tunneling current density J_T can be ignored as compared with the thermionic current density given by Eq. (8).

III. THERMIONIC EMISSION FROM GRAPHENE

In Fig. 2(a), the thermionic emitted current density J based on Eq. (8) is plotted as a function of temperature T (log-log scale) for various $\Phi = 3$, 4, and 5 eV (solid lines) at fixed $E_F = 0.083$ eV, and $v_f = 10^6$ m/s. The results based on the RD law are also presented (dashed lines) for comparison. Here, we assume that the work function does not change with the temperature. For a given work function, a scaling of T^3 is predicted by our model, which is different from the traditional RD scaling of T^2. In the inset, we plot $\ln(J/T^3)$ (left y axis for our model) and $\ln(J/T^2)$ (right y axis for the RD law) versus $1/T$ for work functions = 3–5 eV.

In Fig. 2(b), we compare the analytical formula Eq. (8) (red line) with the numerical solution of Eq. (7) (circles) up to $T = 2500$ K (at $E_F = 0.083$ eV and $\Phi = 4.514$ eV). The comparison shows good agreement up to $T = 200$ K. The deviation at a higher temperature is due to the approximation of the Maxwell-Boltzmann distribution to the Fermi-Dirac distribution in solving the integral. This comparison implies that Eq. (8) is accurate up to 2000 K (a practical temperature).

In Fig. 3(a), the thermionic current density J [from Eq. (8)] is calculated as a function of T (up to 2000 K) for various Fermi energy levels $E_F = 0.083$–0.4 eV. From the figure, we see that increasing E_F can drastically enhance J. In order to decrease the temperature to $T = 900$–1000 K with $J > 10\ \mathrm{A/m^2}$, it is required to have a higher $E_F =$ 0.8–0.9 eV and also a lower work function $\Phi = 2.5$ or 3 eV as shown in Fig. 3(b). Note that the calculated J is sensitive at around $E_F = 0.8$ and 0.9 eV and $\Phi = 2.5$–3 eV. For example, if we use lower $E_F = 0.8$ eV and higher $\Phi = 3$ eV, J is significantly reduced to $J < 1\ \mathrm{A/m^2}$ [see the inset in Fig. 3(b)]. It is worth noting that the Fermi level can be tuned experimentally over a wide range (0.5–0.85 eV) via different methods such as chemical doping [35] and electrostatic gate voltage [36]. Some recent studies also suggest that graphene can be engineered to have a lower work function (2.5–3 eV) [37].

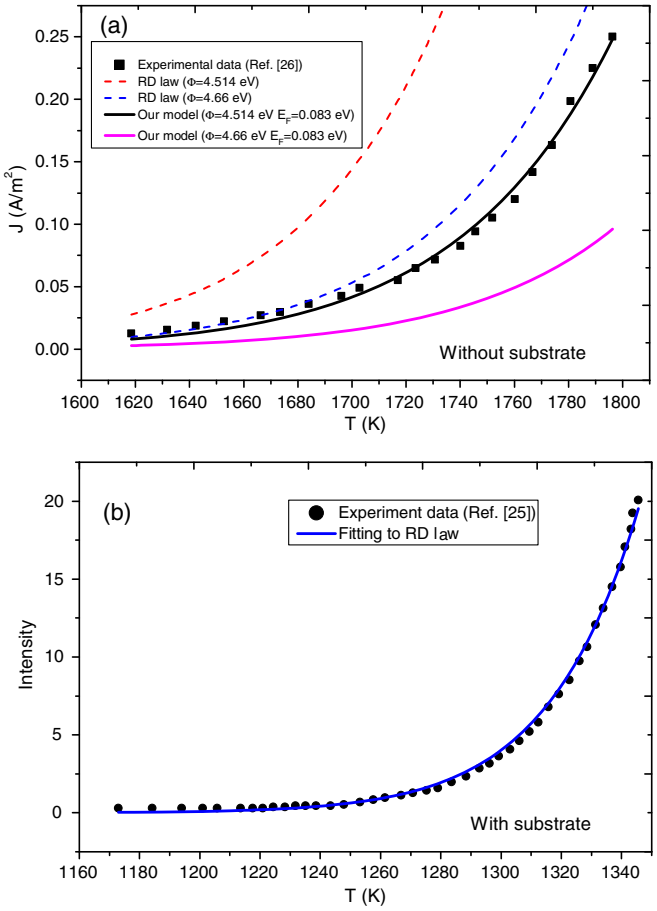

FIG. 4. (a) A comparison of our calculated results (black solid line, 4.514 eV; magenta solid line, 4.66 eV) and of the RD law (blue dashed line, 4.66 eV; red dashed line, 4.514 eV) with experimental results Ref. [26] (black square) for electron emission from single-layer suspended graphene (no substrate effect). From the experiment, the emission area of graphene is $5 \times 2.5\ \mathrm{mm^2}$, and the anode voltage (500 V) is separated from the graphene surface by 3.7 mm. The applied F is less than $1\ \mathrm{V}/\mu\mathrm{m}$, so the Schottky lowering effect can be ignored. (b) A comparison with the experimental result Ref. [25] (symbols) and the RD law (line), where the effect of the substrate is important, as the graphene is on top of a metallic substrate.

There is a recent experiment measuring the thermionic electron emission from single-layer graphene (suspended on a CNT film) in the range of $T = 1600$–1750 K (see Fig. 4 in Ref. [26]). In Fig. 4(a), we fit the experimental data (black square symbol) to our model with a work function of about $\Phi = 4.514$ eV and $E_F = 0.083$ eV, which shows better agreement (black solid line) as compared to using the traditional RD law with 4.66 eV for the bulk graphite (dashed blue line). In comparison, the RD law at 4.514 eV (dashed red line) shows much larger values,

and our model at 4.66 eV predicts much lower current values than the experimental data. This extracted work function (4.514 eV) is in excellent agreement with the experimental measured value around 4.5 eV [38] and also the theoretical value by density-functional theory [39]. Theoretically, the reduction of the work function is expected, because when the thickness of bulk graphite is reduced down to single-layer graphene, the quantum size effect in the normal direction becomes very important, then the size-reduction-induced confinement causes the upward shift in electron total energy, and thus the work function of graphene become smaller (see Sec. 4.1 in Ref. [40]).

On the other hand, if the graphene is placed on different metallic substrates, another recent experiment [25] shows that the data are well described by the traditional RD law, as shown in Fig. 4(b). Here, the type of substrate affects the amount of current significantly with a fitted and effective work function (based on the RD law) ranging from 3.3 to 4.6 eV including effects of the substrate [25]. The findings [reported in Figs. 4(a) and 4(b)] indicate that the metallic-based substrate plays an important role for thermionic emission from graphene. Note that the effects of the substrate have been completely ignored in our model, which is beyond the scope of this paper.

IV. TIC

By ignoring other energy losses, we calculate the ideal efficiency η of a TIC in using graphene as a cathode (4.514 eV) at cathode temperature T_c and metallic material as an anode of different work function Φ_a and temperature T_a. The value of η is calculated by

$$\eta = \frac{(J_c - J_a)(\Phi_c - \Phi_a)}{J_c(\Phi_c + 2k_B T_c) - J_a(\Phi_a + 2k_B T_a)}. \qquad (15)$$

Here, we use Eq. (8) to calculate J_c and the RD law for J_a.

Figure 5 shows the calculated η (solid lines) as a function $\Phi_a = 0.5$–4.5 eV for different T_a (K) $= 300$, 500, 800, and 1000 for a fixed graphene cathode property: $T_c = 1800$ K, $\Phi_c = 4.514$ eV, and $E_F = 0.083$ eV. From the figure, we see that, for a given T_a, there is an optimal value of anode work function Φ_a for which the TIC will have a maximal value of $\eta_{\max}$. As an example, we have $\eta_{\max} \approx 0.45$ at $T_a = 800$ K, $T_c = 1800$ K, and $\Phi_a \approx 2.25$ eV (blue line). This behavior remains valid for T_c down to 900 K (see the inset). The maximum efficiency $\eta_{\max}$ (left y axis) and its corresponding optimal values of anode work function Φ_a (right y axis) are plotted in the inset as a function of anode temperature $T_a = 300$–800 K for two cathode temperatures $T_c = 900$ (black dashed lines) and 1800 K (red solid lines). Using this inset, we can immediately know the maximum efficiency $\eta_{\max}$ of the TIC and obtain the required values of T_a and Φ_a. At low $T_c = 900$ K (see the black dashed lines in the inset), we need $T_a \approx 425$ K and $\Phi_a \approx 2.5$ eV to have $\eta_{\max} \approx 0.45$.

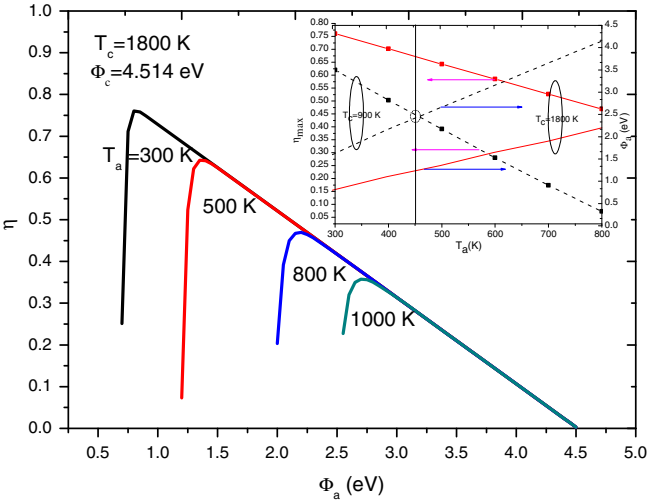

FIG. 5. Efficiency of a graphene-based cathode TIC as a function of the work function of metallic anode Φ_a at four different anode temperatures $T_a = 300$, 500, 800, and 1000 K and fixed cathode temperature $T_c = 1800$ K. The inset gives the maximum efficiency $\eta_{\max}$ (left) and the required Φ_a (right) as a function of T_a at $T_c = 900$ (black) and 1800 K (red).

Note that the most recent work shows that the LaB_6 heterostructure may have a work function around to 2–3 eV [41], and it may be a suitable candidate for the anode material for the proposed high-efficiency TIC shown in Fig. 5.

V. CONCLUSIONS

In summary, we propose to use single-layer graphene as the cathode material in the design of a high-efficiency TIC. In order to provide some quantitative design parameters, we first develop a model to calculate the electron thermionic emission from single-layer suspended graphene by ignoring the effect of the substrate. From our model, an analytical formula [Eq. (8)] is formulated, which is verified with a numerical calculation and compared with experimental results. Our findings suggest that the traditional thermionic emission law governed by the well-known RD equation is no longer valid if the effect of the substrate is not important. Our model predicts a scaling of T^3, which is different from the classical RD scaling of T^2.

By considering that the graphene can be engineered to have a higher Fermi energy (around 0.8–0.9 eV) [35,36], and to have a lower work function (to 2.5–3 eV) [37], it is possible to have a graphene-based cathode to emit a sufficiently high current density (> 10 A/m^2) at $T = 700$–1000 K.

A proposed TIC with single-layer graphene as a cathode (work function $= 4.514$ eV) and a metallic electrode as an anode of a different work function is designed for which the optimal anode work function and anode temperature are calculated to obtain a maximal efficiency. It is possible to have a TIC at an efficiency of about 45% with a cathode

temperature of 900 K and with a metallic anode of about 2.5 eV work function (like the LaB_6 anode) at around 425 K. These findings may shed light on developing a thermionic cathode using graphene and also a thermal-energy-harvesting device like the TIC. The work is also useful in the development of materials with a low work function, like the LaB_6 heterostructure with a lowering work function of 0.46 eV [41].

ACKNOWLEDGMENTS

The authors thank Dr. Peng Liu and Professor Kaili Jiang for helpful discussion and kindly providing us with their original experimental data. In addition, we are also grateful for the referee's constructive comments on the manuscript. This work is supported by SUTD (SRG EPD 2011 014) and SUTD-MIT IDC Grant (IDG21200106 and IDD21200103). L. K. A. acknowledges the support of AFOAR AOARD Grant No. 14-2110.

[1] O. W. Richardson, *Thermionic Emission from Hot Bodies* (Wexford College Press, London, 2003).
[2] J. L. D. Terence, D. Musho, W. F. Paxton, and D. G. Walker, Quantum simulation of thermionic emission from diamond films, J. Vac. Sci. Technol. B **31**, 021401 (2013).
[3] K. S. Novoselov, A. K. Geim, S. V. Morozov, D. Jiang, Y. Zhang, S. V. Dubonos, I. V. Grigorieva, and A. A. Firsov, Effect in atomically thin carbon films, Nature (London) **306**, 666 (2004).
[4] K. S. Novoselov, A. K. Geim, S. V. Morozov, D. Jiang, M. I. Katsnelson, I. V. Grigorieva, S. V. Dubonos, and A. A. Firsov, Two-dimensional gas of massless Dirac fermions in graphene, Nature (London) **438**, 197 (2005).
[5] A. A. Balandin, S. Ghosh, W. Bao, I. Calizo, D. Teweldebrhan, F. Miao, and C. N. Lau, Superior thermal conductivity of single-layer graphene, Nano Lett. **8**, 902 (2008).
[6] S. Sun, L. K. Ang, D. Shiffler, and J. W. Luginsland, Klein tunneling model of low energy electron field emission from single-layer graphene sheet, Appl. Phys. Lett. **99**, 013112 (2011).
[7] S.-J. Liang, S. Sun, and L. K. Ang, Over-barrier side-band electron emission from graphene with a time-oscillating potential, Carbon **61**, 294 (2013).
[8] S.-J. Liang and L. K. Ang, Chiral tunneling-assisted over-barrier electron emission from graphene, IEEE Trans. Electron Devices **61**, 1764 (2014).
[9] A. C. Walt, A. de Heer, and D. Ugarte, A carbon nanotube field-emission electron source, Science **270**, 1179 (1995).
[10] J.-M. Bonard, M. Croci, C. Klinke, R. Kurt, O. Noury, and N. Weiss, Carbon nanotube films as electron field emitters, Carbon **40**, 1715 (2002).
[11] B. K. Sarker and S. I. Khondaker, Thermionic emission and tunneling at carbon nanotube-organic semiconductor interface, ACS Nano **6**, 4993 (2012).
[12] Y. Cheng and O. Zhou, Electron field emission from carbon nanotubes, C.R. Phys. **4**, 1021 (2003).
[13] S.-D. Liang, N. Y. Huang, S. Z. Deng, and N. S. Xu, Quantum effects in the field emission of carbon nanotubes, J. Vac. Sci. Technol. B **24**, 983 (2006).
[14] S.-D. Liang and L. Chen, Generalized Fowler-Nordheim theory of field emission of carbon nanotubes, Phys. Rev. Lett. **101**, 027602 (2008).
[15] S.-D. Liang and L. Chen, Theories of field and thermionic electron emissions from carbon nanotubes, J. Vac. Sci. Technol. B **28**, C2A50 (2010).
[16] X. Wei, S. Wang, Q. Chen, and L. Peng, Breakdown of Richardson's law in electron emission from individual self-Joule-heated carbon nanotubes, Sci. Rep. **4**, 5102 (2014).
[17] X. Wei, D. Golberg, Q. Chen, Y. Bando, and L. Peng, Phonon-assisted electron emission from individual carbon nanotubes, Nano Lett. **11**, 734 (2011).
[18] H. Yoon, C. Forsythe, N. T. L. Wang, K. Watanabe, T. Taniguchi, J. Hone, P. Kim, and D. Hami, Measurement of collective dynamical mass of Dirac fermions in graphene, Nat. Nanotechnol. **9**, 594 (2014).
[19] M. Zebarjadi, K. Esfarjani, M. Dresselhaus, Z. Ren, and G. Chen, Perspectives on thermoelectrics: From fundamentals to device applications, Energy Environ. Sci. **5**, 5147 (2012).
[20] G. N. Hatsopoulos and E. P. Gyftopoulos, *Thermionic Energy Conversion I* (MIT Press, Cambridge, MA, 1974).
[21] S. Meir, C. Stephanos, T. H. Geballe, and J. Mannhart, Highly-efficient thermoelectronic conversion of solar energy and heat into electric power, J. Renew. Sust. Energy **5**, 043127 (2013).
[22] J. W. Schwede *et al.*, Photon-enhanced thermionic emission from heterostructures with low interface recombination, Nat. Commun. **4**, 1576 (2013).
[23] J. W. Schwede *et al.*, Photon enhanced thermionic emission for solar concentrator systems, Nat. Mater. **9**, 762 (2010).
[24] G. Segev, Y. Rosenwaks and A. Kribus, Loss mechanisms and back surface field effect in photon enhanced thermionic emission converters, J. Appl. Phys. **114**, 044505 (2013).
[25] E. Starodub, N. C. Bartelt, and K. F. McCarty, Viable thermionic emission from graphene-covered metals, Appl. Phys. Lett. **100**, 181604 (2012).
[26] F. Zhu, X. Lin, P. Liu, K. Jiang, Y. Wei, Y. Wu, J. Wang, and S. Fan, Heating graphene to incandescence and the measurement of its work function by the thermionic emission method, Nano Res. **7**, 1 (2014).
[27] P. R. Wallace, The band theory of graphite, Phys. Rev. **71**, 622 (1947).
[28] A. H. C. Neto, F. Guinea, N. M. R. Peres, K. S. Novoselov, and A. K. Geim, The electronic properties of graphene, Rev. Mod. Phys. **81**, 109 (2009).
[29] E. L. Murphy and J. R. H. Good, Thermionic emission, field emission, and the transition region, Phys. Rev. **102**, 1464 (1956).
[30] X. Wei, Q. Chen, and L. Peng, Electron emission from a two-dimensional crystal with atomic thickness, AIP Adv. **3**, 042130 (2013).
[31] W. R. Smythe, *Static and Dynamic Electricity* (McGraw-Hill, New York, 1950).
[32] J. G. Simmons, Generalized formula for the electric tunnel effect between similar electrodes separated by a thin insulating film, J. Appl. Phys. **34**, 1793 (1963).

[33] W. S. Koh and L. K. Ang, Quantum model of space-charge-limited field emission in a nanogap, Nanotechnology **19**, 235402 (2008).

[34] D. C. Wood, University of Kent Computing Laboratory, Technical Report No. 15-92, 1992.

[35] G. Giovannetti, P. A. Khomyakov, G. Brocks, V. M. Karpan, J. van den Brink, and P. J. Kelly, Doping graphene with metal contacts, Phys. Rev. Lett. **101**, 026803 (2008).

[36] X. Gan *et al.*, High-contrast electrooptic modulation of a photonic crystal nanocavity by electrical gating of graphene, Nano Lett. **13**, 691 (2013).

[37] M. Petrovic *et al.*, The mechanism of caesium intercalation of graphene, Nat. Commun. **4**, 2772 (2013).

[38] K. Xu *et al.*, Direct measurement of Dirac point energy at the graphene/oxide interface, Nano Lett. **13**, 131 (2013).

[39] C. Christodoulou *et al.*, Tuning the work function of graphene-on-quartz with a high weight molecular acceptor, J. Phys. Chem. C **118**, 4784 (2014).

[40] W. T. Zheng and C. Q. Song, Underneath the fascinations of carbon nanotubes and graphene nanoribbons, Energy Environ. Sci. **4**, 627 (2011).

[41] J. Voss, A. Vojvodic, S. H. Chou, R. T. Howe, and F. Abild-Pedersen, Inherent enhancement of electronic emission from hexaboride heterostructure, Phys. Rev. Appl. **2**, 024004 (2014).